Chapter 2
Newly Identified Star Clusters in M33: Space-Based Survey

Hiltner (1960) present photometry of 23 M33 cluster candidates and 23 M31 globular clusters using photographic plates at the 2.5 m Mt. Wilson Telescope. Since this early study, it was established that, in general, clusters in M33 are bluer and fainter than those in M31. There have been a number of M33 cluster catalogs published since this pioneer work. The most comprehensive catalog of extended objects in M33 was compiled by Christian and Schommer (1982, 1988). They present a catalog of 250 nonstellar objects including photometry of 106 star cluster candidates. More recently, Mochejska et al. (1998) detect 51 star clusters candidates, of which 32 were not previously cataloged. With the arrival of the HST, studies of the M33 star clusters have rapidly increased (Bedin et al. 2005; Chandar et al. 1999a, b, c, 2002). Ma et al. (2001, 2002a, b, c, 2004a, b) obtained ages of M33 star clusters using spectral energy distributions in 13 intermediate filters of the Beijing-Arizona-Taiwan-Connecticut (BATC) photometric system. The reader is referred to the work of Sarajedini and Mancone (2007) (hereafter SM), which merged all of the modern catalogs compiled before 2007, for a summary of the properties of all of these catalogs. Even the results of Park and Lee (2007), which appeared after the publication of SM have been incorporated into the web-based version of the SM catalog.[1]

This master catalog contains 479 candidates of which 264 are confirmed clusters based on HST and high resolution ground-based imaging. The most recent work in this field is that of Zloczewski et al. (2008, hereafter ZKH), which presents a catalog of 4780 extended sources in a 1 square degree region around M33 including 3554 new candidate stellar clusters. For the purpose of the present project, it is important to take special note of the two cluster catalogs by Chandar et al. (1999a, 2001, hereafter CBF99, CBF01 or collectively as CBF) and the one by Sarajedini et al. (2006) because we will adopt similar reduction and analysis techniques as these previous studies.

In general, ground-based imaging cannot clearly distinguish a star cluster from another type of extended source (e.g. nebula, galaxy), but Hubble Space Telescope (HST) imaging with the Wide-Field Planetary Camera 2 (WFPC2) or the Advanced

[1] http://www.astro.ufl.edu/~ata/cgi-bin/m33_cluster_catalog/index.cgi

I. San Roman, *The Formation and Evolution of M33 as Revealed by Its Star Clusters*, Springer Theses, DOI: 10.1007/978-1-4614-7327-5_2,

Camera for Surveys (ACS) provides the spatial resolution necessary to provide an unequivocal determination. It is for this reason that we have undertaken the present study. In addition, and just as importantly, the HST observations allow us to construct color-magnitude diagrams (CMDs) of the star clusters, which can be used to estimate ages and investigate any correlations that might exist between cluster ages and integrated photometric properties as well as allowing us to determine star cluster masses. Section 2.1 describes the observations and data reduction, and Sect. 2.2 discusses the identification and integrated magnitudes of the clusters. Section 2.2.2 includes a statistical analysis of the most recent previous survey of M33 clusters by Zloczewski et al. (2008). The analysis of the CMDs is presented in Sect. 2.3 while an analysis of the star cluster properties is in Sect. 2.4. Lastly, Sect. 2.5 presents our conclusions.

2.1 Observations and Data Reduction

The observations for the present study were obtained with the Advanced Camera for Surveys Wide Field Channel (ACS/WFC) onboard the Hubble Space Telescope (HST). With a pixel scale of $0.049''$ pixel^{-1} and a field of view of $3.3' \times 3.3'$, ACS/WFC is able to resolve individual stars at the distance of M33. Twelve HST/ACS fields from the GO-10190 program (PI: D. Garnett) have been analyzed. Four primary fields were obtained along the major axis of M33. Eight coordinated parallel fields were also secured along both sides of the primary-field axis. Figure 2.1 shows the locations of these fields. We have three filters for the primary observations (F475 W, F606 W, F814 W) and two filters for the parallel images (F606 W, F814 W). Table 2.1 presents a summary of the observations.

All of the images were calibrated through the standard pipeline-process and downloaded from the HST archive. The 'FLT' images (Table 2.1), which were used for the point source photometry, were first multiplied by the geometric correction image to correct for the fact that each ACS pixel subtends a different angle on the sky. Then, the data quality files were applied by setting the values of bad pixels to a large negative number so that the photometry software will ignore them. The photometry was performed using the DAOPHOT/ALLSTAR and ALLFRAME routines (Stetson 1994) following the same procedure as that used by Sarajedini et al. (2000). A detailed description of how the point spread functions (PSFs) were constructed has been presented in Sarajedini et al. (2006). The corresponding frames in the F606 W and F814 W filters were matched to obtain mean instrumental magnitudes of common stars which were then matched to form colors. The photometry has been corrected for the charge transfer efficiency (CTE) problem that ACS suffers using the prescription of Riess and Mack (2004). In addition, the theoretical transformation of Sirianni et al. (2005) was used in order to convert the magnitudes to the ground-based Johnson-Cousins system.

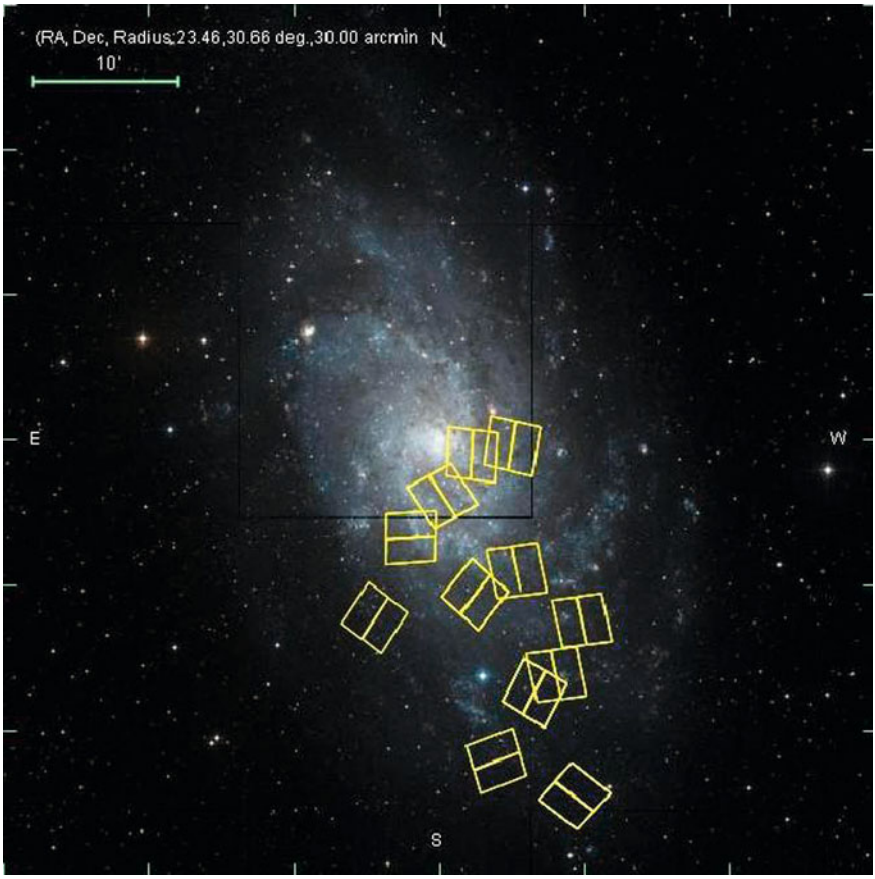

Fig. 2.1 Location of our observed ACS/WFC fields overplotted on an image of M33. North is *up* and east is to the *left*

The pipeline-processed drizzled ('DRZ') images were used for the integrated cluster photometry and were similarly obtained from the HST archive. In fields where multiple drizzled images were produced by the pipeline, we derived positional offsets between these frames using the imshift and imcombine tasks in IRAF to allow us to produce one master image per filter per field. The drizzling process removes the sky background and corrects the counts to an exposure time of one second. As a result, to make the calculation of photometric errors more straightforward, each DRZ image was multiplied by the exposure time and the background sky value was added back before performing photometry on these frames. The resultant images were then used in the derivation of the integrated cluster photometry.

Table 2.1 Observation summary

Field	R.A. (J2000.0)	Decl. (J2000.0)	Filter	Exp. time (s)
D1	01 33 49.89	+30 35 48.12	F606 W	2 × 2480, 1 × 1300, 1 × 120
			F814 W	2 × 2480, 1 × 1522, 1 × 142
			F475 W	3 × 700
D2	01 33 39.69	+30 28 59.98	F606 W	8 × 2480, 1 × 1300, 1 × 120
			F814 W	10 × 2480, 1 × 1500, 1 × 120
			F475 W	3 × 700
D3	01 33 20.49	+30 22 14.99	F606 W	8 × 2480, 1 × 1300, 1 × 120
			F814 W	10 × 2480, 1 × 1500, 1 × 120
			F475 W	3 × 700
D4	01 33 07.89	+30 15 06.98	F606 W	8 × 2480, 1 × 1300, 1 × 120
			F814 W	10 × 2480, 1 × 1500, 1 × 120
			F475 W	3 × 700
F1	01 33 40.32	+30 38 39.89	F606 W	1 × 2160
			F814 W	1 × 2160
F2	01 33 27.52	+30 39 15.42	F606 W	1 × 2400
			F814 W	1 × 2500
F3	01 34 00.23	+30 32 56.43	F606 W	1 × 2400
			F814 W	1 × 2500
F4	01 33 26.04	+30 30 37.64	F606 W	1 × 2160
			F814 W	1 × 2160
F5	01 34 11.78	+30 27 21.94	F606 W	1 × 2160
			F814 W	1 × 2160
F6	01 33 05.39	+30 27 11.88	F606 W	1 × 2400
			F814 W	1 × 2500
F7	01 33 13.43	+30 23 29.64	F606 W	1 × 2160
			F814 W	1 × 2160
F8	01 33 32.92	+30 17 32.37	F606 W	1 × 2400
			F814 W	1 × 2400

2.2 Cluster Identification and Photometry

Star clusters are easily resolved on the HST/ACS images so the selection of objects has been done by visual inspection of each image. This is the technique employed in several previous papers where HST imaging was used (CBF, Sarajedini et al. 2006). Figure 2.2 shows sample images of some of the 161 clusters identified in this study. The cluster positions have been determined by convolving each image with an elliptical gaussian of $\sigma = 10$ pixels. This kernel size was chosen so that the convolution process would yield a smooth cluster profile that is conducive to the next step, which is the application of the IRAF imexamine task. This routine was applied to the smoothed cluster profiles to determine the cluster centers. The optimum pixel coordinate positions were transformed to right ascension and declination using the World Coordinate System in the image headers. Based on the work of SM, which compared the positional accuracy of several catalogs with those determined using

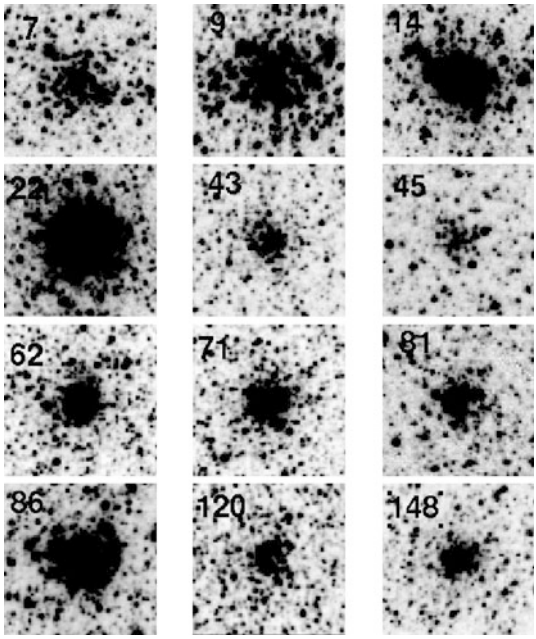

Fig. 2.2 Representative sample of star clusters present in our fields in the F606 W filter. Each image is shown with the same gray-scale intensity and 5″ on a side, with north *up* and east to the *left*

the Local Group Survey images of Massey et al. (2006), we estimate an internal precision of approximately ±0.1 arcsec and an absolute accuracy of about ±0.4 arcsec for these quoted cluster positions.

The integrated magnitudes and colors of each cluster have been calculated using the aperture photometry routines in DAOPHOT (Stetson 1987). To be consistent with the previous work of Sarajedini et al. (2006), we have adopted an aperture radius of 2.2″ for the magnitude measurements and 1.5″ for the colors. Note that CBF used the same aperture size for their magnitudes but a variable aperture ranging from 1.0″ to 2.2″ within which to measure cluster colors. Like in the CBF study, the background sky is always determined in an annulus with an inner radius of 3.5″ and an outer radius of 5.0″. Once again, these magnitudes have been corrected for CTE based on Riess and Mack (2004) and calibrated to the ground-based system using the synthetic transformations of Sirianni et al. (2005).

Table A.1 in Appendix A details the position of each cluster as well as its V magnitude, B−V color, V−I color, reddening, age, mass and also, if applicable, the alternative identification in Sarajedini and Mancone (2007). We could not determine the integrated magnitudes for two of the clusters because of their location near the edge of the field. The formal random errors on the magnitudes and colors are all less than 0.01 mag because of the high signal-to-noise ratio of these clusters. Cluster candidates number 139 and 59 in the catalog of Sarajedini and Mancone (2007) have been rejected as clusters in this study based on visual inspection.

2.2.1 Comparison with Previous Photometry

Comparing our results with the CBF study, we find a mean difference of $<V(Us - CBF)> = 0.09 \pm 0.06$ and $<(V - I)> = 0.07 \pm 0.03$ while comparing with Ma et al. (2001, 2002a, c), we arrive at a difference of $<V(Us - Ma)> = 0.04 \pm 0.05$, where the uncertainties are standard errors of the mean. As we shall see below, these photometric differences are not unexpected for integrated photometry of extended objects such as star clusters (see also Table 2 of Sarajedini and Mancone 2007). Figure 2.3 shows the offset in magnitude and color in both cases. The integrated B magnitudes are not plotted due to a lack of significant numbers of clusters with which to compare.

In order to examine these results in more detail, we analyzed the magnitude and color offsets as a function of field and position. Not surprisingly, the mean difference is larger in fields and positions near the center of the galaxy as a result of the higher degree of crowding. Analysis of the distance distribution of our sample reveals that 50 % of the CBF clusters with measured V magnitudes are inside a distance of 1.7 kpc from the center of M33. The mean magnitude difference for the clusters inside this region is $<V(Us - CBF)> = 0.17 \pm 0.07$ while for those outside this region, the difference is $<V(Us - CBF)> = 0.02 \pm 0.09$. Examining different distance ranges, moving progressively outward to include more CBF clusters, we find the same tendency where clusters in the inner (more crowded) regions display a larger mean magnitude difference as compared with the outer (less crowded) regions.

It is important to note that we also performed additional tests of the photometry to investigate the effects of spatial resolution and errors in cluster centering. The CBF photometry comes mostly from the Wide Field (WF) CCDs that are part of the WFPC2 onboard HST. The spatial resolution of the WF CCDs is roughly 4 times coarser as compared with ACS/WFC. We performed photometry of a subset of our clusters using ACS/WFC images that were resampled to replicate the

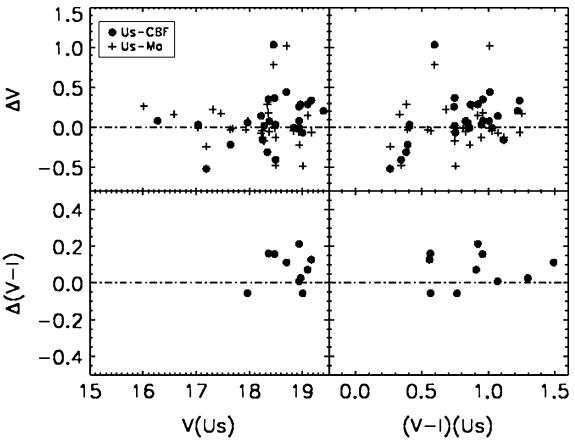

Fig. 2.3 Comparison of the integrated cluster photometry from the present study with that of CBF and Ma et al. (2001, 2002a, c)

resolution of the WF CCDs. We found no significant difference between these results and the magnitudes as measured on the original ACS/WFC frames.

Additionally, we analyzed the sensitivity of our photometry to the adopted cluster center by using the values from the Sarajedini and Mancone (2007) catalog, which are measured from ground-based images taken from the Local Group Survey using the MOSAIC instrument as well as from the work of CBF. Again, we find no significant difference in the magnitudes and colors of the clusters we have measured.

A further check of our photometry is provided by the realization that, as shown in Fig. 2.1, several of our fields exhibit significant overlap. There are 10 clusters that have multiple measurements of their magnitudes and colors: one common cluster between d2 and f4, five between f1 and f2 and four between d3 and f7. Comparing the photometry of these common clusters, we obtain an offset in V magnitude of $V = 0.042 \pm 0.026$ and an offset in color of $(V - I) = 0.060 \pm 0.012$.

At first glance, this level of disagreement between measurements of the same clusters in different fields seems to be a potential cause for concern. However, an examination of a similar situation encountered by CBF99 and CBF01 reveals that their studies show offsets of the same order. In particular, as pointed out by SM, there are 3 clusters in common between CBF99 and CBF01, and these objects appear on two different WFPC2 fields. The mean difference in the V mags of these clusters is $\Delta V(\text{CBF99} - \text{CBF01}) = 0.106 \pm 0.048$.

2.2.2 Comparison with Previous Catalogs

As noted previously, the SM catalog is the pre-eminent compilation containing all of the existing information for M33 star clusters up to 2007. Of the 161 clusters identified in the present work, 46 have been previously cataloged in Sarajedini and Mancone (2007). Figure 2.4 shows the integrated magnitude CMD for all of the genuine clusters in the SM catalog. We see that the clusters span a magnitude range of $16 < V < 20$, which corresponds to $-9 < M_V < -5$, using our adopted distance modulus of $(m - M)_0 = 24.69$ (Galleti et al. 2004). Figure 2.4 also illustrates the locations of the clusters identified in the present study. This new sample extends to $M_V \sim -4$, which is ~ 1 mag fainter than the least luminous clusters in the SM catalog, closer to the faintest clusters in the Large Magellanic Cloud (Sarajedini and Mancone 2007).

We can also compare our cluster catalog with the most recent catalog produced by Zloczewski et al. (2008, hereafter ZKH); they present a photometric survey for stellar clusters in M33 based on deep ground-based images obtained with the MegaCam instrument on the Canada-France-Hawaii telescope, and their classifications are based on visual inspection of the images. Their catalog contains 4780 extended sources in a region approximately $1^\circ \times 1^\circ$. Among these, there are 3554 new candidate stellar clusters of which 122 are relatively bright, likely globular clusters.

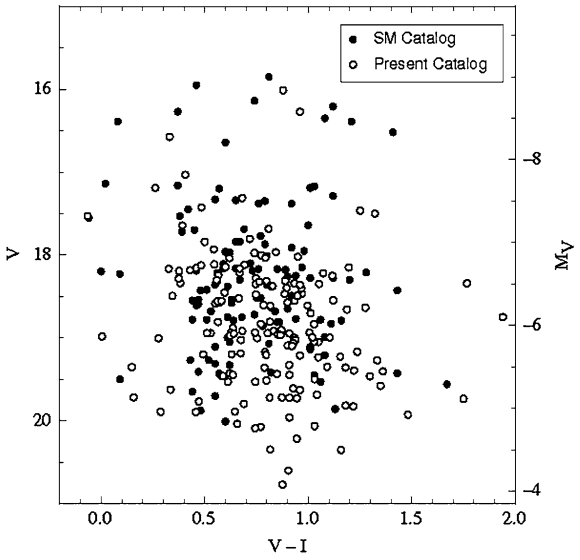

Fig. 2.4 Color-magnitude diagram of the genuine M33 clusters from the SM catalog (*filled circles*) as compared with those from the present study (*open circles*). The distribution of the two types of points is largely similar except that the present catalog contains more faint star clusters than that of SM. The faintest clusters here have MV ∼–4.0 rivaling the faintest globular clusters in the Milky Way and populous clusters in the LMC

Sixty of the 3554 objects are present in our HST/ACS fields. The ZKH catalog suggests that 51 of these are new candidate stellar clusters; however our study shows that only 21 objects resolve into stars and therefore appear to be clusters. Some of the other objects that ZKH consider to be extended turn out to be close groupings of two or three stars. Others appear to be background galaxies or diffuse nebulae. Table 2.2 provides a cross-identification of the 21 common objects that are genuine clusters. If we extrapolate the ratio of true clusters to total cluster candidates in the ZKH catalog, this suggests that only around 40 % of the 3554 proposed candidates from ZKH will be actual stellar clusters. Nonetheless, even if there are ∼1400 stellar clusters in M33, it would have the highest number of known star clusters per unit luminosity of any spiral galaxy in the Local Group.

2.3 Color-Magnitude Diagrams

Intrinsic properties such as age, metallicity and reddening govern the integrated magnitudes and colors of clusters. Using the PSF-photometry of each star in each field we are able to examine these parameters by constructing CMDs of each cluster. Figure 2.5 shows the radial CMD and the best fit-isochrone for cluster 7 as an example of the procedure we followed. The top-left to the bottom-right in the left panel correspond to stars within 1″ of the cluster center, between 1″ and 2″, 2″ and 3″ and finally between 3″ and 4″. The solid lines represent theoretical isochrones from Girardi et al. (2000) for ages of 10^8, 10^9 and 10^{10} years with a metallicity of Z = 0.004. This metal abundance has been chosen as a representative mean of the disk abundance gradient based on the work of Kim et al. (2002, see also Sarajedini et al. 2006). However, we

Table 2.2 Cross identification with Zloczewski et al. (2008)

ID (ZKH)	ID (US)	R.A. (J2000.0)	Decl. (J2000.0)	Notes	Type[a]
25-1-009	1	1 32 59.38	30 26 54.12	…	0
25-1-008	2	1 32 59.95	30 27 19.57	…	0
25-1-003	5	1 33 02.39	30 26 55.71	…	0
25-1-001	6	1 33 02.98	30 26 34.56	…	0
34-2-001	7	1 33 03.29	30 16 02.26	…	1
33-4-018	9	1 33 05.62	30 14 23.44	…	1
33-5-022	12	1 33 08.93	30 16 51.53	…	0
33-6-016	14	1 33 09.77	30 22 35.46	…	1
33-5-019	16	1 33 10.38	30 15 45.93	…	0
33-6-014	17	1 33 12.14	30 22 36.97	…	1
33-6-010	18	1 33 12.95	30 23 07.14	Small	0
33-5-014	20	1 33 13.96	30 14 31.85	…	0
33-5-013	21	1 33 14.04	30 15 16.47	Small	0
33-6-009	23	1 33 14.71	30 23 19.05	…	1
33-6-008	24	1 33 15.22	30 21 14.07	…	0
33-6-006	25	1 33 16.10	30 20 56.55	…	2
33-3-021	27	1 33 19.16	30 23 22.62	…	1
33-3-020	30	1 33 21.31	30 20 31.88	…	0
33-2-010	47	1 33 25.73	30 18 01.12	…	0
33-2-003	69	1 33 32.88	30 15 46.76	…	0
32-5-024	77	1 33 36.38	30 15 32.61	…	0

Note Units of RA are hours, minutes, and seconds, and units of Dec are degrees, arcminutes, and arcseconds

[a] Proposed classification in ZKH: −1 galaxy, 0 unclassified, 1 likely stellar cluster and 2 an already known high confidence cluster included in Sarajedini and Mancone (2007)

point out that for ages younger than ∼1 Gyr, there is very little sensitivity of the isochrone-derived age on the assumed metal abundance. The isochrones have been shifted by a distance modulus of $(m - M)_0 = 24.69$ (Galleti et al. 2004) and a line-of-sight reddening value of $E(V - I) = 0.06$ (Sarajedini et al. 2000). Then, we overplot the isochrones in the observed CMDs looking for the best fit to the main sequence turnoff (MSTO) region. Based on Cardelli et al. (1989), we adopt the following relation between the extinction and the reddening: $A_I = 1.3 \cdot E\,(V-I)$.

The left panel illustrates the gradual decrease in cluster stars at increasing distance from the cluster center. Consequently, CMDs within 1″ of the cluster center display a significant fraction of stars belonging to the cluster revealing features to estimate ages, while the lower panels have been used to monitor non-cluster stars. Right panel in each figure shows the best fit-isochrone for stars within 1″ of the cluster center. In this way, the ages of 148 star clusters have been estimated from a comparison of the main-sequence turnoff photometry with theoretical isochrones. In some cases, an additional reddening adjustment was needed in order to align the main sequence of the isochrones with the data. In several instances, the main sequence and the turnoff are not satisfactorily defined to permit

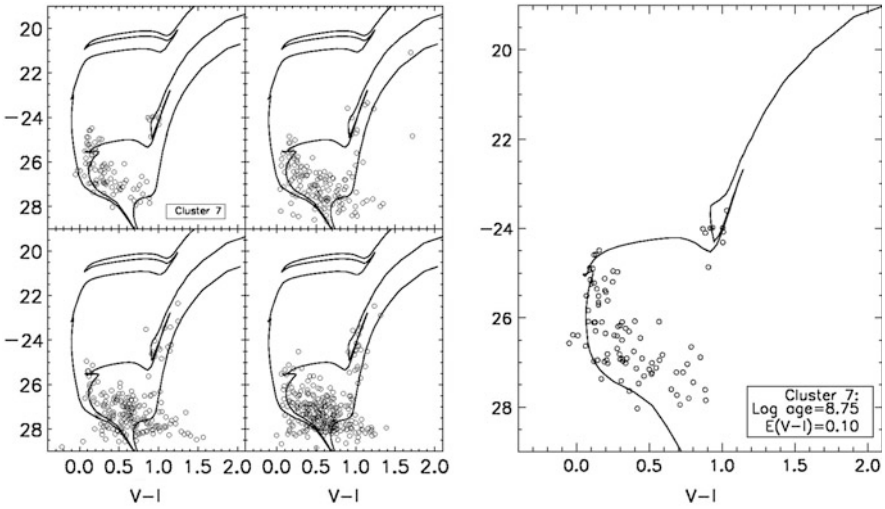

Fig. 2.5 *Left Panel* CMD for the region around cluster 7. The *top left panel* shows the stars within 1″ of the cluster center, the *top right panel* includes the stars between 1″ and 2″, while the stars between 2″ and 3″ and 3″ and 4″ are displayed in the *bottom right panel* and the *bottom left*, respectively. The *solid lines* correspond to isochrones from Girardi et al. (2000) for ages of 10^8, 10^9 and 10^{10} years and a metallicity of Z = 0.004. *Right Panel* The best fit-isochrone for stars within 1″ of the cluster center

a comparison with isochrones. We estimate a precision in the isochrone-fitting ages of ±0.05 dex based on neighboring isochrones (in age) that could also potentially fit the data. In the case of clusters 12, 15, 18 and 111, the isochrone fit is not as well established and the precision of the age reaches 0.1 dex. The precision of the reddenings is approximately ±0.05 mag. The ages and reddenings obtained during this process are listed in Table A.1 in Appendix A.

2.4 Analysis

The reddening-corrected colors of the clusters should correlate with their ages and metallicities. The upper panel of Fig. 2.6 shows the variation of integrated cluster V − I color with the estimated isochrone age. These have been reddening corrected using the reddening listed in Table A.1. The lines are the expected relations according to simple stellar populations Girardi et al. (2002) with Z = 0.004 (solid line), Z = 0.001 (dotted line) and Z = 0.019 (dashed line). As expected, this plot reveals a positive correlation between cluster age and V − I color in much the same manner as the models predict.

Our data allow us to compare the luminosities of the clusters with their ages in order to derive the cluster masses. The bottom panel of Fig. 2.6 shows the integrated absolute magnitudes as a function of the estimated isochrone ages. These

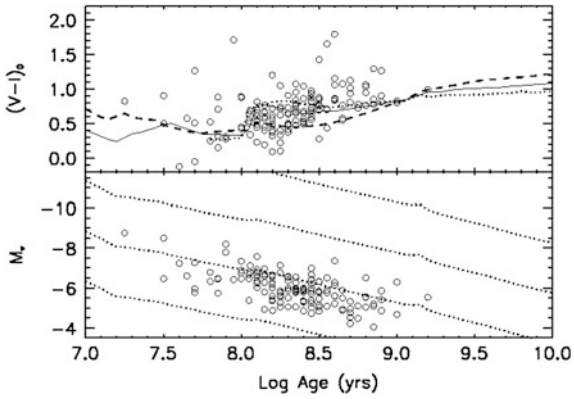

Fig. 2.6 The *top panel* shows the variation of the clusters' integrated $(V - I)_0$ colors with age. The correction for reddening has been effected using the reddening values obtained in the isochrones fitting process. The *lines* represent the expected relations for a simple stellar population from Girardi et al. (2002) with $Z = 0.004$ (*solid line*), $Z = 0.001$(*dotted line*) and $Z = 0.019$ (*dashed line*). The *lower panel* shows the extinction corrected absolute magnitude as a function of cluster age. The *dashed lines* are the expected relations for a simple stellar population from Girardi et al. (2002) with $Z = 0.004$ and masses of 10^3, 10^4, 10^5 and 10^6 $M_\odot$

have been corrected using an extinction based on the reddening listed in Table A. 1. The dashed lines are the expected relations for simple stellar populations with $Z = 0.004$ taken from Girardi et al. (2002) for masses of 10^3, 10^4, 10^5 and 10^6 $M_\odot$ and assuming a Salpeter initial mass function (IMF). This diagram indicates that the clusters in our sample are consistent with the theoretical predictions of simple stellar population fading models. Additionally, the majority of the clusters have masses between 5×10^3 and 5×10^4 $M_\odot$. These estimated masses would not change significantly if we were to assume other power-law IMFs in constructing the fading lines (Tantalo 2005) although we should consider them as upper limits in other cases like exponential IMFs (Chabrier 2001) and binary-corrected IMFs (Kroupa 1998). It should be noted that the dearth of clusters older than $\sim 10^9$ years is attributable to the fact that our CMDs are generally not deep enough to detect the main sequence turnoffs of clusters older than this limit.

2.5 Summary: Newly Identified Star Clusters

This chapter presents HST/ACS integrated photometry of 161 star clusters in M33 as well as individual stellar photometry in twelve fields. Forty-six clusters of the sample have been previously cataloged by Sarajedini and Mancone (2007). Color-magnitude diagrams of each cluster have been constructed in order to determine ages via isochrone fitting. Simple stellar population models reproduce the behavior of the cluster ages with dereddened $V - I$ color as well as with absolute magnitude.

We have incorporated these new clusters into the existing catalog of M33 clusters established by Sarajedini and Mancone (2007) increasing by more than 40 % the set of confirmed star clusters in this galaxy.

References

Bedin LR, Piotto G, Baume G, Momany Y, Carraro G, Anderson J, Messineo M, Ortolani S (2005) A&A 444:831
Cardelli JA, Clayton GC, Mathis JS (1989) ApJ 345:245
Chabrier, G. 2001, ApJ 554:1274
Chandar R, Bianchi L, Ford HC (1999a) ApJS 122:431
Chandar R, Bianchi L, Ford HC (2001) A&A 366:498
Chandar R, Bianchi L, Ford HC (1999b) ApJ 517:668
Chandar R, Bianchi L, Ford HC, Salasnich B (1999c) PASP 111:794
Chandar R, Bianchi L, Ford HC, Sarajedini A (2002) ApJ 564:712
Christian CA, Schommer RA (1982) ApJS 49:405
Christian CA, Schommer RA (1988) AJ 95:704
Galleti S, Bellazzini M, Ferraro, FR (2004) A&A 423:925
Girardi L, Bertelli G, Bressan A, Chiosi C, Groenewegen MAT, Marigo P, Salasnich B, Weiss A (2002) A&A 391:195
Girardi L, Bressan A, Bertelli G, Chiosi C (2000) A&AS 141:371
Hiltner WA (1960) ApJ 131:163
Kim M, Kim E, Lee MG, Sarajedini A, Geisler D (2002) AJ 123:244
Kroupa P (1998) in Astronomical Society of the Pacific Conference Series, Vol. 134, Brown Dwarfs and Extrasolar Planets, ed. R. Rebolo, E. L. Martin, & M. R. Zapatero Osorio,483–+
Ma J, Zhou X, Chen J (2004a) A&A 413:563
Ma J, Zhou X, Chen J (2004b) ChJAAp 4:125
Ma J, Zhou X, Chen J, Wu H, Jiang Z, Xue S, Zhu J (2002a) AJ 123:3141
Ma J, Zhou X, Chen J, Wu H, Kong X, Jiang Z, Zhu J, Xue S (2002b) AcA 52:453
Ma J, Zhou X, Chen J-S, Wu H, Jiang Z-J, Xue S-J, Zhu J (2002c) Chin J Astron Astrophys 2:197
Ma J, Zhou X, Kong X, Wu H, Chen J, Jiang Z, Zhu J, Xue S (2001) AJ 122:1796
Massey P, Olsen KAG, Hodge PW, Strong SB, Jacoby GH, Schlingman W, Smith RC (2006) AJ 131:2478
Mochejska BJ, Kaluzny J, Krockenberger M, Sasselov DD, Stanek KZ (1998) Acta Astron 48:455
Park W-K, Lee MG (2007) AJ 134:2168
Riess A, Mack J (2004) (Baltimore:STScI), http://www.stsci.edu/hst/acs/documents/isrs/isr0406.pdf
Sarajedini A, Barker MK, Geisler D, Harding P, Schommer R (2006) AJ 132:1361
Sarajedini A, Geisler D, Schommer R, Harding P (2000) AJ 120:2437123
Sarajedini A, Mancone, CL (2007) AJ 134:447
Sirianni M, Jee MJ, Benítez N, Blakeslee JP, Martel AR, Meurer G, Clampin M, De Marchi G, Ford HC, Gilliland R, Hartig GF, Illingworth GD, Mack J, McCann WJ (2005) PASP 117:1049
Stetson PB (1987) PASP 99:191
Stetson PB (1994) PASP 106:250
Tantalo R (2005) New database of SSPs with different IMFs. In: Corbelli E, Palla F, Zinnecker H (eds) The Initial Mass Function 50 Years Later. Astrophysics and space science library, vol 327, p 235. http://adsabs.harvard.edu/abs/2005ASSL..327..235T. Provided by the SAO/NASA Astrophysics Data System
Zloczewski K, Kaluzny J, Hartman J (2008) Acta Astronomica 58:23

http://www.springer.com/978-1-4614-7326-8

The Formation and Evolution of M33 as Revealed by Its Star Clusters

San Roman, I.

2013, XVI, 129 p., Hardcover
ISBN: 978-1-4614-7326-8